

Φ^4 Oscillatons

Susana Valdez-Alvarado* and L. Arturo Ureña-López†

Departamento de Física, DCI, Campus León, Universidad de Guanajuato, 37150, León, Guanajuato, México

Ricardo Becerril‡

*Instituto de Física y Matemáticas, Universidad Michoacana de San Nicolás de Hidalgo. Edificio C-3,
Cd. Universitaria, 58040, Morelia, Michoacán, México*

(Dated: May 29, 2022)

We solve numerically the Einstein-Klein-Gordon system with spherical symmetry, for a massive real scalar field endowed with a quartic self-interaction potential, and obtain the so-called Φ^4 -oscillatons which is the short name for oscillating soliton stars. We analyze numerically the stability of such oscillatons, and study the influence of the quartic potential on the behavior of both, the stable (S-oscillatons) and unstable (U-oscillatons) cases under small and strong radial perturbations.

PACS numbers: 04.40.-b,04.25.D-,95.30.Sf,95.35.+d

I. INTRODUCTION

Oscillatons are non-singular and asymptotically flat solutions of the Einstein-Klein-Gordon (EKG) equations, in which both metric and scalar field are fully time-dependent[1–5]. They can be considered as gravitationally bounded objects made of a real scalar field in the classical regime, and were first discovered by Seidel and Suen[1]. Oscillatons should be distinguished from their complex counterparts, the so-called boson stars, for which the space-time geometry remains static[6–9]. In the literature we can find other works describing these bound objects and their stability properties[10–16]. Also there have been many works about numerical evolution of scalar fields in different cosmological and astrophysical context[17–19].

Ref. [3] presented an exhaustive study of oscillatons for the simplest case of a massive, non-self interacting, scalar field. It is shown in there that, as in the case of boson stars, oscillatons can be classified into stable (S-branch) and unstable (U-branch) configurations. S-oscillatons are stable configurations under small radial perturbations, and they typically migrate to other S-profiles if strongly perturbed. On the other hand, U-oscillatons are intrinsically unstable: they migrate to the S-branch if their mass is moderate, but they may collapse into black holes if their mass is large enough.

The case of oscillatons with a self-interaction term in the scalar field potential remains without study. This is in contrast to the case of boson stars, whose properties are well known even in the self-interacting case[8, 9, 20]. It is the main purpose of this paper to cover this omission, and to study the properties of self-interacting oscillatons. For that we make use of techniques and methods

that parallel those used in boson star studies and for non-interacting oscillatons[3, 20, 21], which will ease the comparison between the two types of scalar objects.

A summary of the paper is as follows. In Sec. II, we present the equations motion of the self-interacting scalar field. In Sec. III we show the results of the equilibrium configuration and their representative properties, for different values of the self-interaction parameter. In Sec. IV we present the results of the dynamical evolution of oscillatons, and the separate analysis of (stable) S-oscillatons and (unstable) U-oscillatons. Finally, Sec. V is devoted to overall conclusions.

II. MATHEMATICAL BACKGROUND

The action that describes our self-gravitating system is

$$I = \int d^4x \sqrt{-g} \left(\frac{R}{16\pi G} - \frac{1}{2} g^{\alpha\beta} \Phi_{,\alpha} \Phi_{,\beta} + V(\Phi) \right), \quad (1)$$

where $V(\Phi)$ is the scalar potential,

$$V(\Phi) = \frac{1}{2} m_\Phi^2 \Phi^2 + \frac{1}{4} \lambda \frac{\Phi^4}{4}, \quad (2)$$

m_Φ denotes the mass of the scalar field, and λ is the quartic interaction parameter. We shall be interested in the spherically symmetric case for which the metric is written as

$$ds^2 = -\alpha^2(t, x) dt^2 + a^2(t, x) dr^2 + r^2 (d\theta^2 + \sin^2 \theta d\psi^2), \quad (3)$$

where $a(t, r)$ is the radial function, and $\alpha(t, r)$ is the lapse function.

A. Evolution Equations

The energy-momentum tensor for the scalar field $\Phi(t, r)$ endowed with a scalar field potential $V(\Phi)$ is de-

* svaldez@fisica.ugto.mx

† lurena@fisica.ugto.mx

‡ becerril@ifm.umich.mx

defined as

$$T_{\mu\nu} = \Phi_{,\mu}\Phi_{,\nu} - \frac{1}{2}g_{\mu\nu} \left[\Phi^{,\sigma}\Phi_{,\sigma} + m_{\Phi}^2\Phi^2 + \frac{1}{2}\lambda\Phi^4 \right]. \quad (4)$$

We can identify the Klein-Gordon (KG) equation with the conservation equations of the scalar field energy-momentum tensor,

$$T^{\mu\nu}{}_{;\nu} = \Phi^{,\mu} \left(\square\Phi - \frac{dV}{d\Phi} \right) = 0, \quad (5)$$

where $\square = (1/\sqrt{-g})\partial_{\mu}(\sqrt{-g}\partial^{\mu})$ is the d'Alembertian operator. Following Ref. [3], we introduce the first order variables

$$\Psi = \Phi', \quad \Pi = a\dot{\Phi}/\alpha, \quad (6)$$

in order to write appropriate evolution equations for the scalar fields. Hereafter, a prime denotes derivative with respect to r , and a dot denotes derivative with respect to t . The KG equation is then represented by the following set of first order differential equations

$$\dot{\Phi} = \frac{\alpha}{a}\Pi, \quad (7a)$$

$$\dot{\Pi} = \frac{1}{x^2} \left(\frac{x^2\alpha\Psi}{a} \right)' - a\alpha(\Phi + \Lambda\Phi^3), \quad (7b)$$

$$\dot{\Psi} = \left(\frac{\alpha\Pi}{a} \right)'. \quad (7c)$$

As for the metric functions, we will use the so-called Hamiltonian constraint for the radial function,

$$\frac{a_{,x}}{a} = \frac{1-a^2}{2x} + \frac{x}{4} \left[\Pi^2 + \Psi^2 + a^2 \left(\Phi^2 + \frac{1}{2}\Lambda\Phi^4 \right) \right], \quad (8)$$

and the polar-areal slicing condition for the lapse function,

$$\frac{\alpha_{,x}}{\alpha} = \frac{a^2-1}{x} - a^2x \left(\frac{\Phi^2}{2} + \frac{1}{4}\Lambda\Phi^4 \right) + \frac{a_{,x}}{a}. \quad (9)$$

For numerical purposes, in all the above equations, we have introduced the dimensionless quantities $r = x/m_{\Phi}$, $t \rightarrow t/m_{\Phi}$, $\Phi \rightarrow \Phi/\sqrt{\kappa_0}$, and $\Lambda \equiv \lambda/(8\pi Gm_{\Phi}^2)$. Eqs. (7-9) are the total set of evolution equations we shall use to explore the properties of self-interacting oscillatons.

III. EQUILIBRIUM CONFIGURATION

Before we evolve the EKG equations, we turn our attention to equilibrium configurations of the self-interacting oscillatons. For that, we consider momentarily a different set of variables: $A(t, x) = a^2$, and $C(t, x) = a^2/\alpha^2$. In terms of these variables, the Einstein equations, $G_{\alpha\beta} = 8\pi T_{\mu\nu}$, read

$$\dot{A} = xA\dot{\Phi}\Phi', \quad (10a)$$

$$A' = \frac{xA}{2} \left[C\dot{\Phi}^2 + \Phi'^2 + A \left(\Phi^2 + \frac{1}{2}\Lambda\Phi^4 \right) \right] - \frac{A}{x}(1 - 10b)$$

$$C' = \frac{2C}{x} \left[1 + A \left(x^2 \left[\frac{1}{2}\Phi^2 + \frac{1}{4}\Lambda\Phi^4 \right] - 1 \right) \right], \quad (10c)$$

whereas the KG is the single equation

$$\Phi'' = C\ddot{\Phi} + \dot{C}\dot{\Phi} - \frac{\Phi'}{x} \left[1 + A \left(1 - x^2 \left[\frac{1}{2}\Phi^2 + \Lambda\frac{1}{4}\Phi^4 \right] \right) \right] + A(\Phi + \Lambda\Phi^3). \quad (11)$$

The above equations will be solved by introducing in Eqs. (10) and (11), the following Fourier expansions for the scalar field and the metric functions,

$$\Phi(t, x) = \sum_{j=1}^{J_{max}} \phi_{2j-1}(x) \cos((2j-1)\omega t) \quad (12a)$$

$$A(t, x) = \sum_{j=0}^{J_{max}} A_j(x) \cos(2j\omega t) \quad (12b)$$

$$C(t, x) = \sum_{j=0}^{J_{max}} C_j(x) \cos(2j\omega t) \quad (12c)$$

where ω is called the fundamental frequency, and J_{max} is the mode at which the Fourier series are truncated. We define $C = C\Omega^{-2}$, with $\Omega = \omega/m_{\Phi}$.

After some lengthy but straightforward algebra, we obtain first-order differential equations for the coefficients A_0 , C_{2j} , Φ_{2j-1} and Ψ_{2j-1} , where $\Psi_{2j-1} = \Phi'_{2j-1}$. This system of equations can be solve with the aid of an integrator, like *odeint*, that uses an adaptive step-size control which allows us to achieve some predetermined accuracy in the solution with minimum computational effort (see [22]). We also use a second order *Runge-Kutta* method (RK2) in order to verify the convergence of our code, since this method uses a fix step-size. Once the profiles of A_0 and Φ_{2j-1} are known, we will get the subsequent values of A_{2j} , for $j \neq 0$, from the algebraic restriction (10a).

A. Boundary Conditions

Appropriate boundary conditions can be obtained by analyzing the regularity of the functions $A(t, x)$, $C(y, x)$, and $\Phi(t, x)$ at $x \rightarrow 0$. First, we realize that $A(t, x=0) = 1$, which implies $A_0(x=0) = 1$, and $A_j(x=0) = 0$ for $j \geq 1$. Second, we find that $\Phi'(t, x=0) = 0$, so that $\phi'_j(x=0) = 0 \forall j$.

From asymptotic flatness, we know that $A(t, x \rightarrow \infty) = 1$, which leads to $A_0(x \rightarrow \infty) = 1$, and $A_j(x \rightarrow \infty) = 0$ for $j \geq 1$. The scalar field must vanish when $x \rightarrow \infty$, and this implies $\phi_j(x \rightarrow \infty) = 0 \forall j$. Likewise, we expect $C(t, x \rightarrow \infty) = \Omega^2$, and then $C_0(x \rightarrow \infty) = \Omega^2$, whereas $C_j(x \rightarrow \infty) = 0$ for $j \geq 1$. Actually, the fundamental frequency Ω is always an output value obtained after the solution of Eqs. (10b), (10c), and (11).

Note that there are not boundary conditions for $C_j(x)$ and $\phi_j(x)$ at $x = 0$. We need to find these values in such manner that all boundary conditions at $x \rightarrow \infty$ are satisfied. For each solution, we will fix the value of the first scalar Fourier coefficient $\phi_1(0)$, and adjust the

rest of the coefficients $\phi_{j \leq 2}$ and $C_{j \geq 0}$ until we satisfy the boundary conditions[2]; we use a non-linear shooting method to find these values. Thus, we obtain a set of eigenvalues for each value $\phi_1(0)$, which in turn defines uniquely a given configuration.

B. Numerical Results

We truncate the Fourier expansions (12) at $J_{max} = 2$. Then, according to what we said about boundary conditions, we need to calculate the value of the coefficients C_0 , C_2 , C_4 , and ϕ_3 , for each value of the Λ parameter. Table I contains the values obtained once the boundary conditions were satisfied at $x_{max} = 30$ for the fixed value $\phi_1(0) = 0.28$.

	$\Lambda = 0.0$	$\Lambda = 1.0$	$\Lambda = 2.0$	$\Lambda = 3.0$
$C_0(0)$	8.98e-01	8.91e-01	8.88e-01	8.84e-01
$C_2(0)$	6.90e-05	1.16e-05	1.36e-05	3.54e-05
$C_4(0)$	2.66e-06	7.32e-06	9.11e-06	1.68e-05
$\phi_3(0)$	5.77e-07	3.69e-06	6.85e-06	6.57e-07

TABLE I. Resulting values of the Fourier coefficients C_0 , C_2 , C_4 , and ϕ_3 , see Eqs. (12), after the integration of the equations of motion (10); in all cases, $\phi_1(0) = 0.28$, and $x_{max} = 30$. For completeness, the first column shows the usual, non-interacting, massive case; it can be verified that the values obtained coincide with those reported in[3].

In contrast to the non-interacting case, the increasing of Λ complicates the solution of the equations of motion as we consider larger values of ϕ_1 . As a consequence, in Fig. 2 we observe that, for $\Lambda = 2, 3$, we were able to compute the values of masses and frequencies for scalar field values up to $\phi_1(0) = 0.6$, whereas for $\Lambda = 0, 1$ we could compute up to $\phi_1 = 0.7$. In the same way, as the values of Λ and of $\phi_1(0)$ are increased, we must decrease the size of the numerical domain, represented by x_{max} .

We present in Fig. 1 the results for the metric functions g_{rr} , g_{tt} , and the scalar field Φ , for configurations with $\phi_1(0) = 0.2$ and $t = 0$. This functions were calculated for different values of the parameter Λ . Note that the metric functions are non-singular at the origin and asymptotically flat for large x .

Following [2], the total mass M_T is calculated by the so-called Schwarzschild mass,

$$M_\Phi = \frac{m_{Pl}^2}{m_\Phi} \lim_{x \rightarrow \infty} \frac{x}{2} [1 - A^{-1}(t, x)], \quad (13)$$

and the fundamental frequency Ω is obtained from

$$\Omega_\Phi = \lim_{x \rightarrow \infty} \frac{\sqrt{C(t, x)}}{A(t, x)}. \quad (14)$$

In Fig. 2, we show the values obtained for the total masses and fundamental frequencies as functions of the central value of the first scalar field (Fourier) coefficient

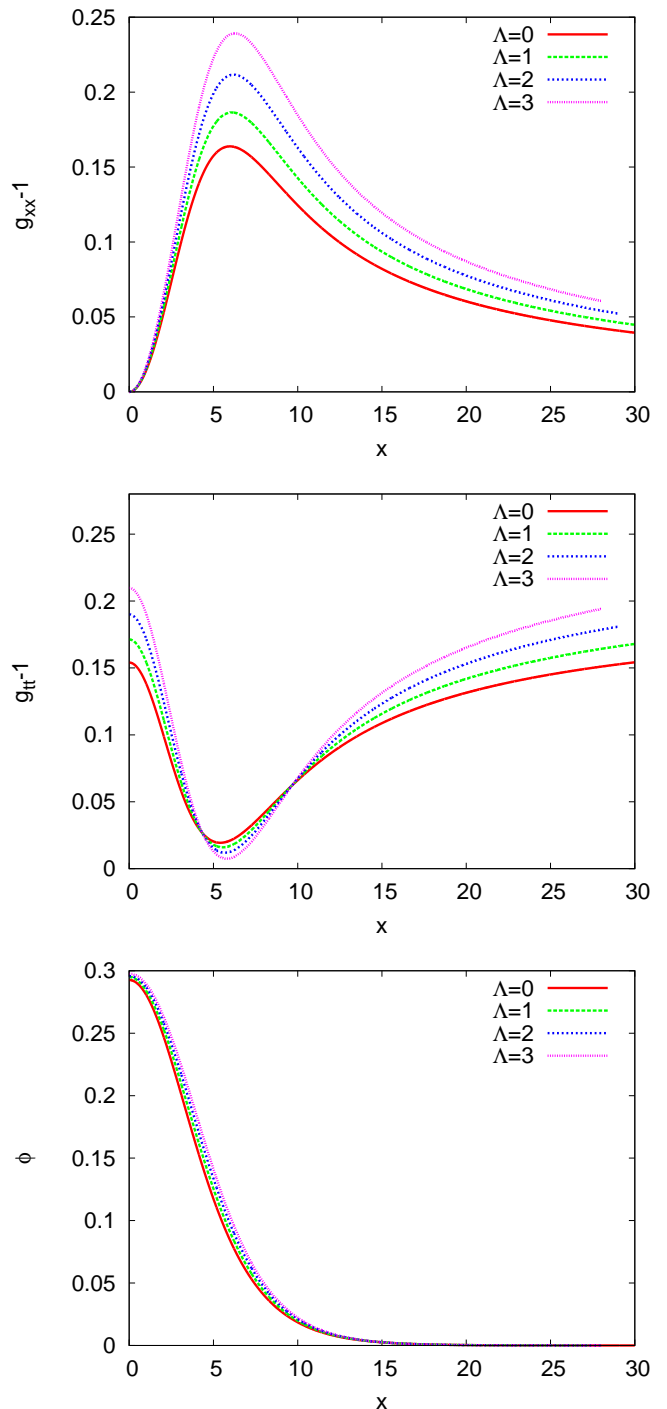


FIG. 1. Metric functions (Top) g_{rr} , (Middle) g_{tt} , and (Bottom) the scalar field Φ of equilibrium configurations corresponding to different values of the quartic parameter Λ . For all examples, we set $\phi = 0.2$, $x_{max} = 30$.

$\phi_1(0)$ and for different values of Λ . We can see that the mass of a given configuration increases for larger values of Λ increases, whereas the fundamental frequency Ω_Φ decreases.

In Table II, we show the values of the fundamental fre-

quency Ω_Φ and of the critical masses M_{Φ_c} for each value of Λ . The critical mass is defined as the maximum mass attained by an equilibrium configuration; this maximum can be seen in Fig. 2 for each value of Λ .

Λ	$M_{\Phi_c}(m_{Pl}^2/m_\Phi)$	$\phi_{1c}(0)$	Ω_Φ
0.0	0.605	0.48	0.862
1.0	0.694	0.47	0.851
2.0	0.770	0.44	0.850
3.0	0.854	0.39	0.848

TABLE II. Resulting values of the critical mass M_{Φ_c} for different Λ 's. As expected, the mass of the equilibrium configurations increase for larger values of Λ , whereas the fundamental frequency decreases. There is also a shift to lower values of the critical value $\phi_{1c}(0)$ as Λ increases.

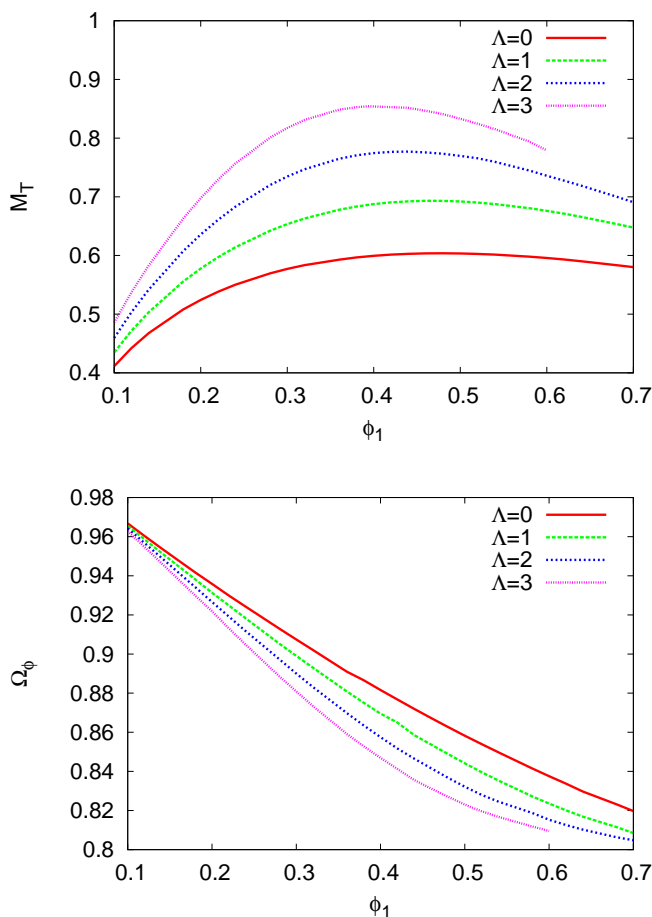


FIG. 2. (Top) M_Φ and (Bottom) Ω_Φ as functions of the central value of the Fourier coefficient $\phi_1(0)$ for different values of Λ . We can observe in that there is a shift to the left of the critical value $\phi_{1c}(0)$, which corresponds to that equilibrium configuration with a critical mass M_{Φ_c} , as Λ increases.

For completeness, we show in Fig. 3, for different equilibrium configurations, the critical mass M_{Φ_c} as a function of the radius R_{max} at which the metric radial function reaches its maximum value at $t = 0$.

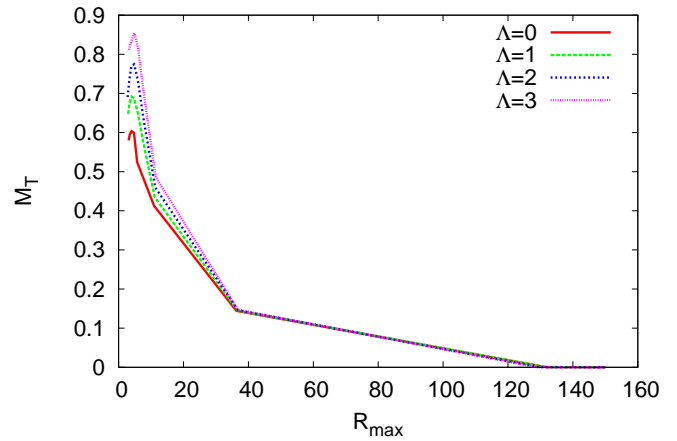


FIG. 3. Typical graph of M_Φ in terms of the maximum radius R_{max} , the radius at which the radial metric function g_{rr} reaches its maximum value, see Fig. 1, for different values of Λ . The configurations become more massive and more compact for larger values of the self-interacting parameter.

IV. NUMERICAL EVOLUTION OF SELF-INTERACTING OSCILLATONS

We proceed now to the evolution of the EKG equations using the method of lines. For the time integrations, we use a fourth order *Runge-Kutta* method (RK4), and second order centered differences to discretize spatial derivatives. A second-order *Runge-Kutta* method (RK2) is used for the spatial integration of the metric functions at each time level. Special care is needed for Eq. (7b), otherwise its discretization would not be second-order accurate because of the presence of the factor $1/x^2$ in the principal part. The transformation that guarantees the accuracy of our simulations at the origin is

$$\Pi_{,t} = 3 \frac{\partial}{\partial x^3} \left(\frac{x^2 \alpha \Psi}{a} \right) - a \alpha (\Phi + \Lambda \Phi^3). \quad (15)$$

A. Boundary Conditions

To properly account for the origin at $x = 0$, we use the fictitious point $x_0 = -\Delta x/2$ as in [3], and take a spatial grid of the form $x_i = (i - 1/2)\Delta x$. From the evolution equation of Φ , Eq. (7a), we can see that it not necessary to apply boundary condition for Φ , because the evolution equation can be integrated all the way from the boundary point $x_0 = -\Delta/2$ up to the outer boundary point. This is possible since the evolution equation (7a) does not have spatial derivatives. Likewise, we use the fictitious point to impose appropriate parity conditions on the scalar field variables: Π is even, and Ψ is odd.

At the outer numerical boundary, we assume that Π behaves as an outgoing wave pulse of the form

$$\Pi = u(x - t)/x, \quad (16)$$

where u is an arbitrary function. In differential form, Eq. (16) becomes

$$\partial_x \Pi + \partial_t \Pi + \Pi/x = 0. \quad (17)$$

By using finite difference in Eq. (17), we can solve it to find the unknown boundary value at the new time level. Because Π behaves as an outgoing wave at the boundary, so does Φ . Then, the outgoing wave boundary condition applied to Φ implies that at the outer boundary

$$\Psi = -\Pi - \Phi/x. \quad (18)$$

We used this expression to obtain boundary values for Ψ after the calculation of those of Φ and Π .

Boundary conditions for the metric functions are the following. Local flatness at the origin implies that $a(x=0) = 1$ and $\partial_x a(x=0) = 0$, and these two conditions together imply that $a(x_0) = a(x_1) = 1 + \mathcal{O}(\Delta x)^3$. We use these two values at the first and second grid points to integrate the second order Hamiltonian constrain outwards to obtain $a(x)$.

As for the lapse function, we impose $\alpha = 1/a$ as an outer boundary condition; this is because in vacuum our slicing condition implies that we are in Schwarzschild coordinates. Then, we are assuming that our boundary conditions are sufficiently far away as to be always in vacuum. Finally, the slicing condition is integrated inwards to obtain the full profile of $\alpha(x)$.

B. Initial Conditions

For most of our numerical experiments, we consider as initial conditions the equilibrium configurations calculated in Sec. III; hence,

$$\Phi(t=0, x) = \sum_{j=1}^{J_{max}} \phi_j(x), \quad (19)$$

$$\Psi(t=0, x) = \Phi'(0, x) = \sum_{j=1}^{J_{max}} \phi'_j(x), \quad (20)$$

$$\Pi(t=0, x) = \dot{\Phi}(0, x) = 0. \quad (21)$$

Our interest resides mainly in the equilibrium properties of these configurations, and it is first necessary to develop different analysis techniques for their study. In this we will include, to begin with, initial configurations that are a deformation of the original equilibrium ones. There is a practical reason behind: equilibrium configurations are easy to evolve, whereas general configurations may be very difficult to follow as they develop in time.

C. Numerical Results

We start by calculating some properties of the equilibrium configurations found now by the evolution code.

Λ	$M_{\Phi_c}(m_{Pl}^2/m_\Phi)$	$\phi_{1c}(0)$
0.0	0.599	0.47
1.0	0.686	0.46
2.0	0.767	0.42
3.0	0.843	0.39

TABLE III. Resulting values of the critical mass M_{Φ_c} for the numerical evolution of equilibrium oscillatons using different Λ 's, see also Table II and text below for details.

For instance, the critical mass M_{Φ_c} of self-interacting oscillatons, for different values of Λ , are shown in Table III.

The total mass was obtained through the integration of the energy density calculated from the time-time component of the scalar field stress-energy tensor, $\rho_\Phi = -T^0_0$. Because of the spherical symmetry, this method gives identical results to the Schwarzschild mass in Eq. (13). We notice a little discrepancy with respect to the values reported in Sec. III, this is because of the evolution code is more accurate and does not depend upon the truncation we had to impose upon the Fourier expansions in (12).

1. Code tests

To revise the accuracy of our numerical calculations, we monitored the momentum constraint (10a),

$$\beta := a_{,t} - \frac{1}{2}x\alpha\Psi\Pi = 0, \quad (22)$$

and calculated the L_2 -norm of the value of β across the grid as a function of time using three different spatial grid sizes, see Fig. 4. It can be seen that the accuracy of the numerical code is not altered by the values of the quartic parameter Λ .

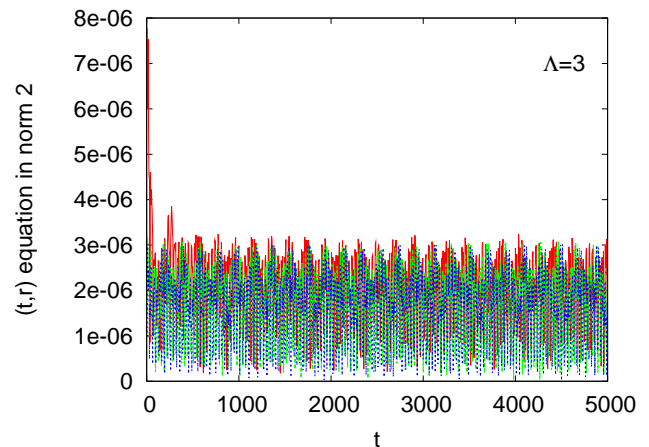


FIG. 4. L_2 -norm of the momentum constraint (10a) for three different resolutions $dx = 0.01$ (red), $dx = 0.02$ (green), 0.04 (blue) and $\Lambda = 3$. It can be seen that the accuracy of the code is kept under control along the runs.

On the other hand, Fig. 5 shows the mass-differential function $x^2\rho$ for a run with a numerical boundary located at $x_{max} = 100$, and for $\Lambda = 3$. We can see that the plots are practically the same up to $x = 20$, but differ one from each other at the outer parts of the numerical domain. These discrepancies, of the order of $x^2\rho < 10^{-5}$, arise because part of scalar field has been reflected from the outer boundary. The error is not significant and we were able to keep it under control during the numerical evolution.

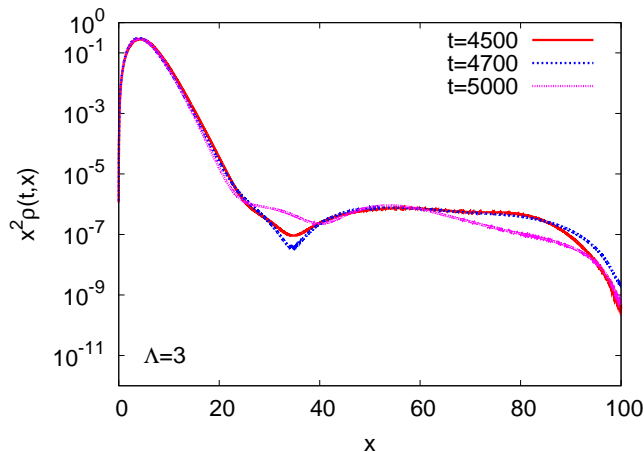


FIG. 5. The function $x^2\rho$ in the case $\Lambda = 3$. The small discrepancies seen at the outer parts of the numerical domain, of the order of $x^2\rho < 10^{-5}$, appear because of the boundary condition used, which is, in the strict sense, only appropriate for the massless case. However, the numerical error is kept under control all along the runs.

Fig. 6 shows the evolution of the total integrated mass for each time level. We can observe a small adjustment of the original mass, because there is a small ejection of scalar field at the beginning of the run. We can notice a steady decay of the mass, which is evidence of an intrinsic dissipation of our numeric code; it can be reduced by taking a finer spatial grid, and then it cannot be considered an intrinsic decay of the oscillatons.

2. S-branch and Quasi-normal Modes

We present here numerical evidence that the characterization of stable, S-branch, and unstable, U-branch oscillatons is preserved in the case of the inclusion of a quartic interaction, much in the same manner as in the case of non self-interacting oscillatons and boson stars.

To begin with, we show in Fig. 7 the evolution of the maximum value of the radial metric function $g_{xx} = a^2(t, x)$, corresponding to an equilibrium configuration with $\phi_1(0) = 0.28$. The outer boundary of the numerical domain was set at $x_{max} = 100$, and the run was followed up to a time $t = 5000$. It can be noticed that the configuration maintains the same oscillatory pattern

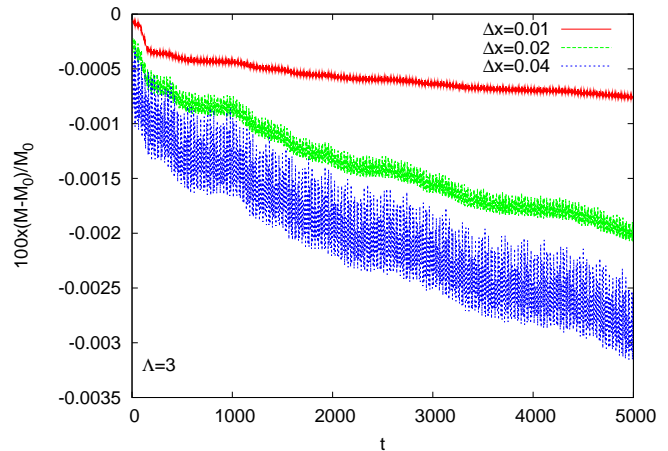


FIG. 6. Typical case of mass dissipation in the numerical evolution of equilibrium configurations. It is caused by the numerical error in the evolution, but we confirmed in our numerical experiments that can be reduced by considering a finer spatial grid.

at all times and for all values of Λ . This is an evidence of the stability of the oscillations in response to small radial perturbations. In this case, the perturbations come from the truncation of the Fourier series (12) and the discretization error of the numerical solutions.

Fig. 8 presents the Fourier transform of the oscillations shown in Fig. 7; we observe that the maximum of the g_{rr} oscillates periodically with two distinctive time scales. The short-period oscillation (large frequency) corresponds to the fundamental frequency used in the Fourier expansions (12). The large-period oscillation (small frequency) is an overall vibration of the configuration that we identify as the characteristic *quasi-normal* modes of the oscillatons.

Following the analysis done in [3], we calculate the power spectrum of the evolution for the entire S-branch; we show in Fig. 9 the quasi-normal frequency f as a function of the total mass M_T . This kind of plots has proved useful in the analysis of the evolution of general scalar field configurations, see[3, 20, 21].

On the other hand, Fig. 10 presents the evolution of the total mass M_T and R_{max} (R_{max} is the value where the radial metric function g_{rr} reaches its maximum value) as compared with the values corresponding to equilibrium configurations. All the cases correspond to the S-branch.

It is observed that slightly perturbed S-oscillatons are not migrating to another S-oscillaton profile, but rather they oscillate with a small amplitude around the original equilibrium configuration. It is then concluded that S-oscillatons are stable under small radial perturbations, and that the frequencies show in Fig. 8 are their intrinsic quasi-normal modes.

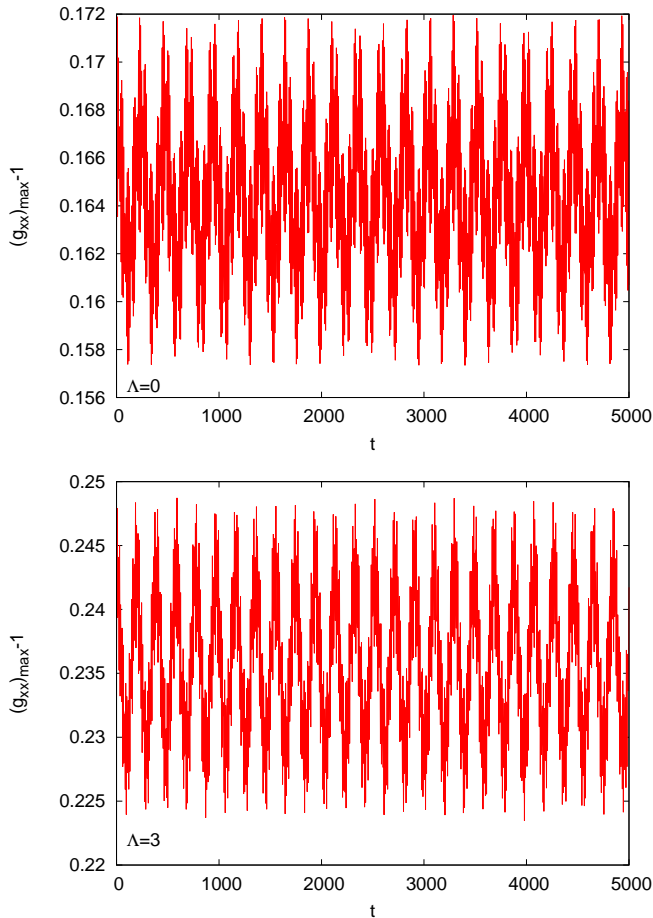


FIG. 7. Maximum value of the radial metric function $g_{rr}(t, x) = a^2(t, x)$, corresponding for the initial configuration $\phi_1(0) = 0.28$ with $\Delta x = 0.01$ and $\Delta t = 0.005$, at $x_{max} = 100$ and the evolution is shown to $t = 5000m^{-1}$ for $\Lambda = 0$ (Top) and 3 (Bottom).

3. Perturbed S-oscillatons

We now turn our attention to the evolution of some strongly-perturbed S-oscillatons. We use a Gaussian profile as a perturbation applied to the original equilibrium configurations; see Fig. 11 for an example of this perturbation in the case of an S-oscillaton with $\phi_1(0) = 0.1$, so that its mass is increased by 40%. The purpose is to analyze whether S-oscillatons are stable under strong perturbations, and the conditions to be met for the collapse into a black hole.

First, we increased the original mass of the equilibrium configuration (see Fig. 2) with $\phi_1(0) = 0.1$ by 40% and 60% for all Λ values. The initial masses for $\Lambda = 1$ are $M_i = 0.5748$ (40%) and $M_i = 0.6816$ (60%), for $\Lambda = 2$ are $M_i = 0.6075$ (40%) and $M_i = 0.7203$ (60%), for $\Lambda = 3$ are $M_i = 0.6423$ (40%) and $M_i = 0.7615$ (60%), and for $\Lambda = 3$ are $M_i = 0.6741$ (40%) and $M_i = 0.8051$ (60%).

From Fig. 12 we can see that for $\Lambda = 0$ the perturbed configuration with its mass increased by 60% collapses

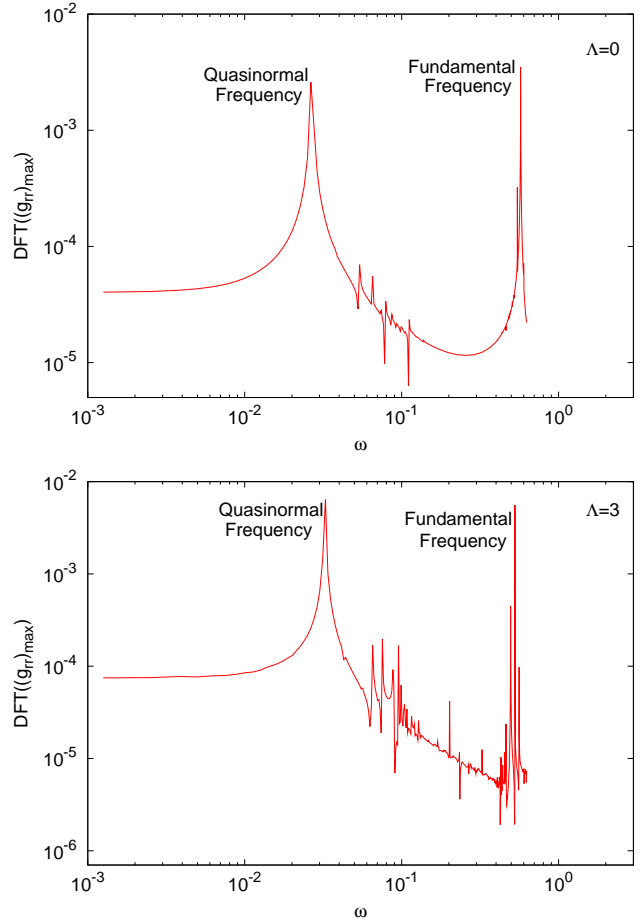


FIG. 8. We show the Fourier transform of the evolution of the maximum value of the metric coefficient g_{rr} for the configuration with $\phi_1 = 0.28$. The corresponding values of the quasi-normal frequencies for the different values of Λ are: $(f/m) = 4.2 \times 10^{-3}$ ($\Lambda = 0$), $(f/m) = 4.8 \times 10^{-3}$ ($\Lambda = 1$), $(f/m) = 5.0 \times 10^{-3}$ ($\Lambda = 2$), $(f/m) = 5.05 \times 10^{-3}$ ($\Lambda = 3$), while their fundamental frequencies are: $(\omega/m) = 0.91$ ($\Lambda = 0$), $(\omega/m) = 0.90$ ($\Lambda = 1$), $(\omega/m) = 0.89$ ($\Lambda = 2$) and $(\omega/m) = 0.88$ ($\Lambda = 3$). Quasi-normal frequencies increase with Λ , a property that can also be noticed in Fig. 7.

into a black hole, while for the rest of the Λ values this configuration migrates to another oscillaton located on the S-branch. The reason for this is that the $\Lambda = 0$ -configuration has an initial mass that is larger than the critical mass of equilibrium configurations (see Table II), whereas for the other cases the initial mass is smaller than the critical one. The perturbed configurations with their mass increased by 40% are able to migrate to another S-oscillaton.

For equilibrium configurations with $\phi_1(0) = 0.2$, we increased its original mass in 25% obtaining the following initial masses: $M_i = 0.6534$ ($\Lambda = 0$), $M_i = 0.7198$ ($\Lambda = 1$), $M_i = 0.7919$ ($\Lambda = 2$), and $M_i = 0.8687$ ($\Lambda = 3$). This configuration collapses into a black hole for all values of Λ ; in all cases, the initial mass of the perturbed

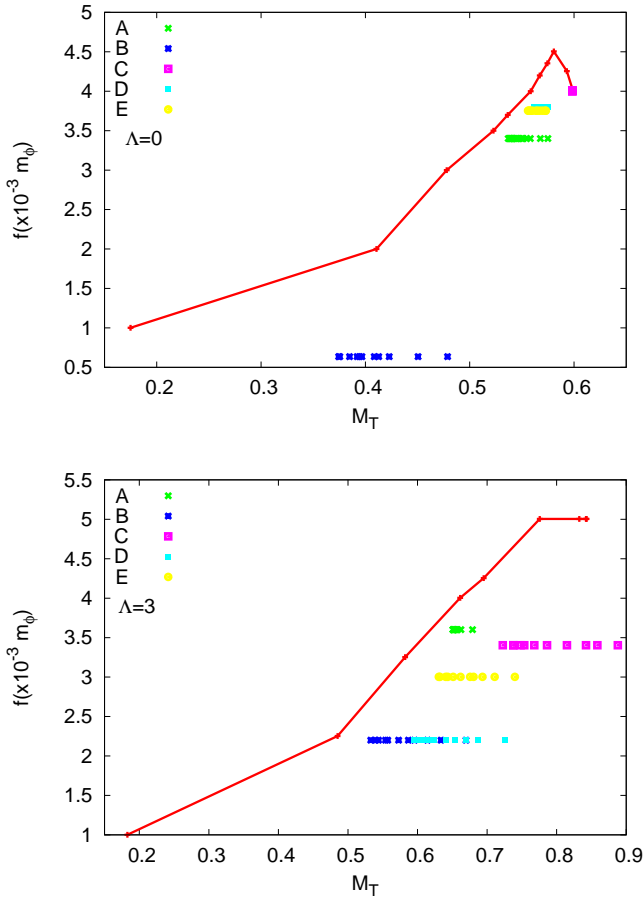


FIG. 9. The quasi-normal frequencies obtained from the evolution of slightly perturbed S-branch oscillatons as a function of the total mass M_T . Also shown is the migration of perturbed S-branch and U-branch oscillatons, labelled A – E, see Figs.

configuration is larger than critical one corresponding to each case.

Finally, for equilibrium configurations with $\phi_1(0) = 0.44$, we decreased its original mass by 20%: $M_i = 0.4787$ ($\Lambda = 0$), $M_i = 0.5484$ ($\Lambda = 1$), $M_i = 0.6133$ ($\Lambda = 2$), and $M_i = 0.6696$ ($\Lambda = 3$). As we can see in Fig. 12, these configurations lose mass until they reach the position of another S-oscillaton.

We have noticed that oscillatons maintain a fixed vibration frequency during its evolution. This is shown in Fig. 12, where we present the migration path of oscillatons with $\phi_1(0) = 0.1$ (with its mass increased by 40%), and with $\phi_1(0) = 0.44$ (with its mass decreased by 20%), which are labeled A and B in Fig. 9. We can appreciate that the perturbed oscillaton with $\phi_1(0) = 0.1$ (+40%) is migrating to an equilibrium configuration with $\phi_1(0) = 0.17$. This can also be seen in Fig. 13, which shows the profile of the metric coefficient g_{rr} rapidly approaching and oscillating around the final configuration.

Then, as reported in Ref. [3], we have found that

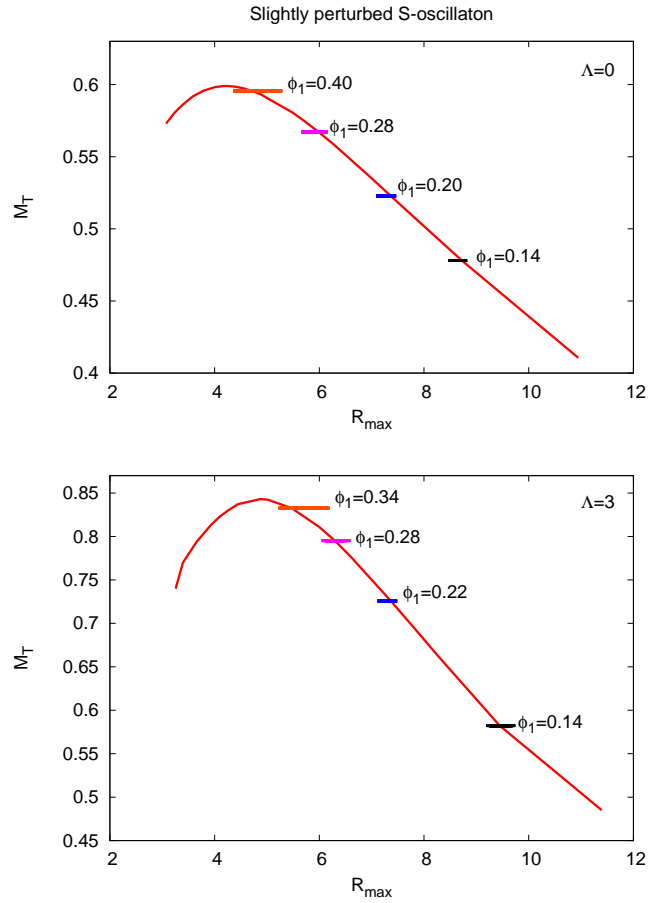


FIG. 10. We show the evolution of the total mass M_T and R_{max} for different slightly-perturbed S-oscillatons up to a time $t = 5000 m^{-1}$. S-oscillatons are not migrating nor decaying, but only oscillating around their equilibrium positions in this plot.

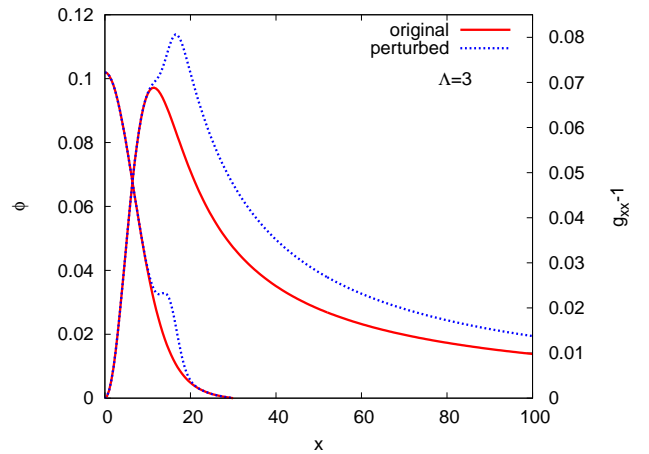


FIG. 11. The scalar field Φ and the radial metric function g_{rr} profiles of a strongly perturbed S-oscillatons with $\phi_1(0) = 0.1$ for the case with a mass increase of 40 percent.

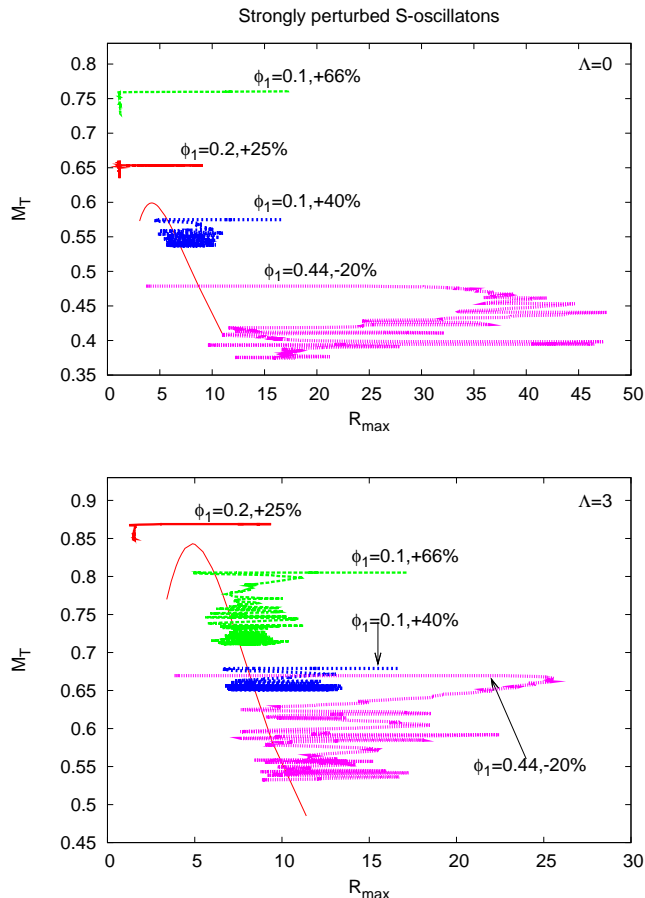


FIG. 12. Evolution of different strongly perturbed S-oscillatons. If the initial mass is less than the critical value M_{Φ_c} , the configurations are able to evolve towards another S-configuration. Otherwise, the final fate may be the collapse into a black hole.

strongly perturbed S-oscillaton are able to migrate to another S-oscillaton when their original mass is smaller than critical mass. But, if the original mass increases enough to be larger than the critical one, this perturbed configuration will collapse into a black hole, except in the case of diluted oscillatons, with low values of ϕ_0 , in which the collapse to a black hole can be prevented by the gravitational cooling mechanism.

4. U-branch

We identify as U-oscillatons the equilibrium configurations that are located on the right-hand side of the critical configuration in a plot of M_T versus $\phi_1(0)$, see Fig. 2, or located on the left-hand side in a plot of M_T versus R_{max} , see Fig. 3. To evolve these equilibrium configurations, we also use the slightly-perturbed, by numerical inaccuracies, configurations, which in general decay and migrate to a configuration located on the S-branch.

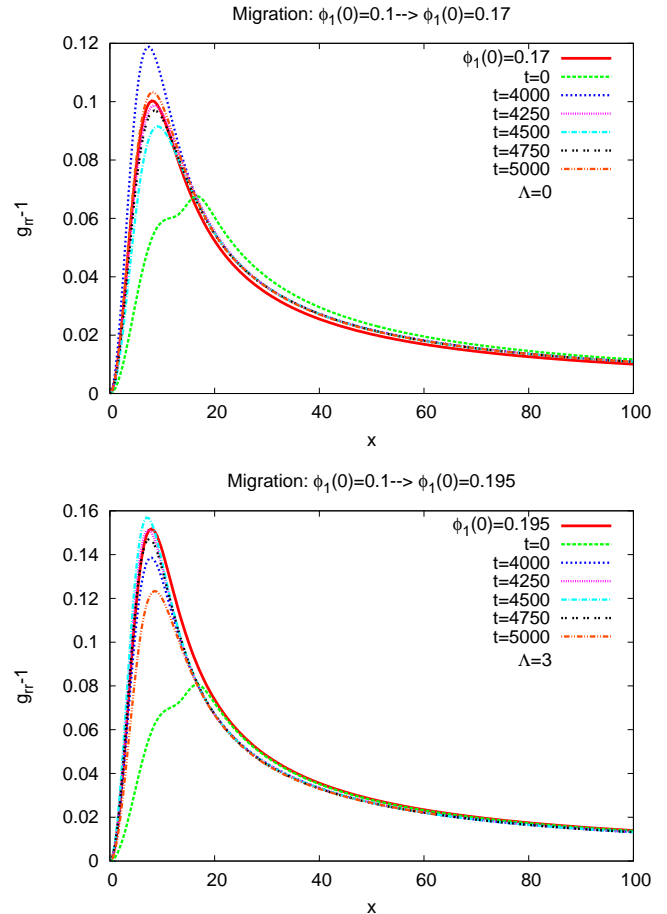


FIG. 13. Evolved profiles of the metric coefficient g_{rr} for a strongly perturbed $\phi_1(0) = 0.1$ -oscillaton for different values of Λ . Each plot indicates the final S-oscillaton each initial configuration is migrating to.

Fig. 14 shows some slightly perturbed U-oscillatons, and we can see that the equilibrium configuration is more unstable (the quicker it starts to migrate) for larger values of $\phi_1(0)$. This also can be seen in Fig. 15, where we show the evolution of the maximum value of the radial metric coefficient g_{rr} for the slightly perturbed configurations with central field values $\phi_1(0) = 0.5$ and $\phi_1(0) = 0.7$.

Thus, we confirm that the U-oscillatons are intrinsically unstable under small perturbation, they decay and migrate to the S-branch. In Fig. 9, we show the migration of the slightly perturbed U-oscillaton with $\phi_1(0) = 0.5$ and $\phi_1(0) = 0.7$, labeled *C* and *E* for $\Lambda = 0$, $\phi_1(0) = 0.7$ labeled *E* for $\Lambda = 1$ and $\Lambda = 2$, and $\phi_1(0) = 0.58$ labeled *E* for $\Lambda = 3$.

5. Perturbed U-branch

We study now the behavior of the U-branch equilibrium configurations under strong perturbations. An ex-

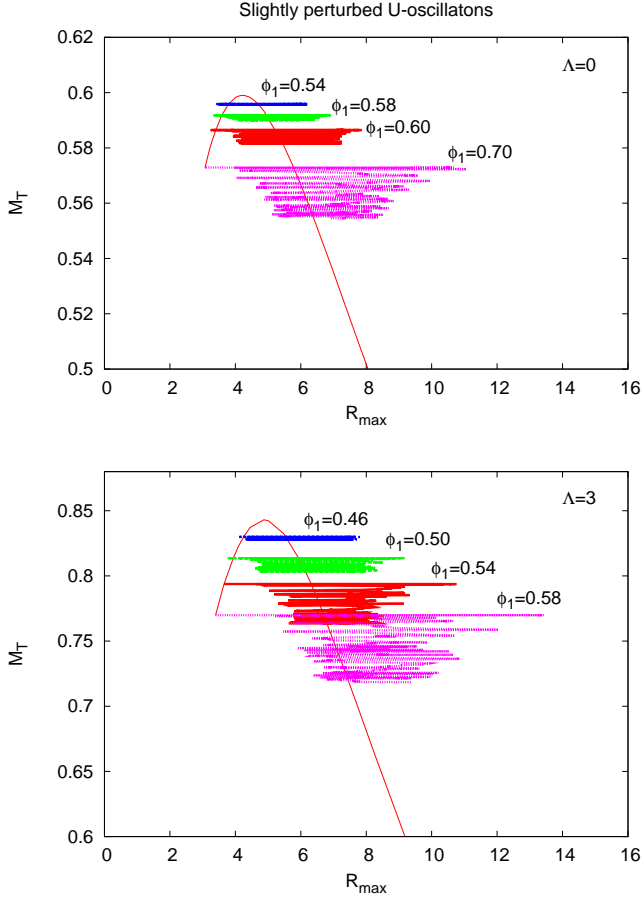


FIG. 14. Slightly-perturbed U-branch configurations. In general, all of them migrate (left to right on the plots) to an equilibrium configuration located on the S-branch.

ample of the typical behaviors is provided by the configuration with $\phi_1(0) = 0.6$ for all values of λ . First, we increase its original mass by 2%; the resulting initial masses are: $M_i = 0.598$ ($\Lambda = 0$), $M_i = 0.678$ ($\Lambda = 1$), $M_i = 0.734$ ($\Lambda = 2$), and $M_i = 0.755$ ($\Lambda = 3$).

In the case of $\Lambda = 0$, this configuration collapses into a black hole, as reported also in [3]. But, for other Λ values, the same configuration is able to migrate to the S-branch, see Fig. 16. The migration path for this configuration is labeled as *C*, for $\Lambda = 1, 2, 3$, in Fig. 9. In contrast, a mass increase by 5% for the equilibrium configuration with $\phi_1(0) = 0.5$ provokes a rapid collapse into a black hole, independently of the value of Λ .

In another experiment, we decrease the original mass of a $\phi_1(0) = 0.6$ -oscillaton by 2%. The initial masses obtained are: $M_i = 0.574$ ($\Lambda = 0$), $M_i = 0.651$ ($\Lambda = 1$), $M_i = 0.706$ ($\Lambda = 2$), and $M_i = 0.725$ ($\Lambda = 3$). As expected, these perturbed U-oscillatons lose mass and migrate to the S-branch. The evolution of these strongly perturbed configurations appears in Fig. 16, and their path migration is labeled as *D* in Fig. 9 for all the values of Λ .

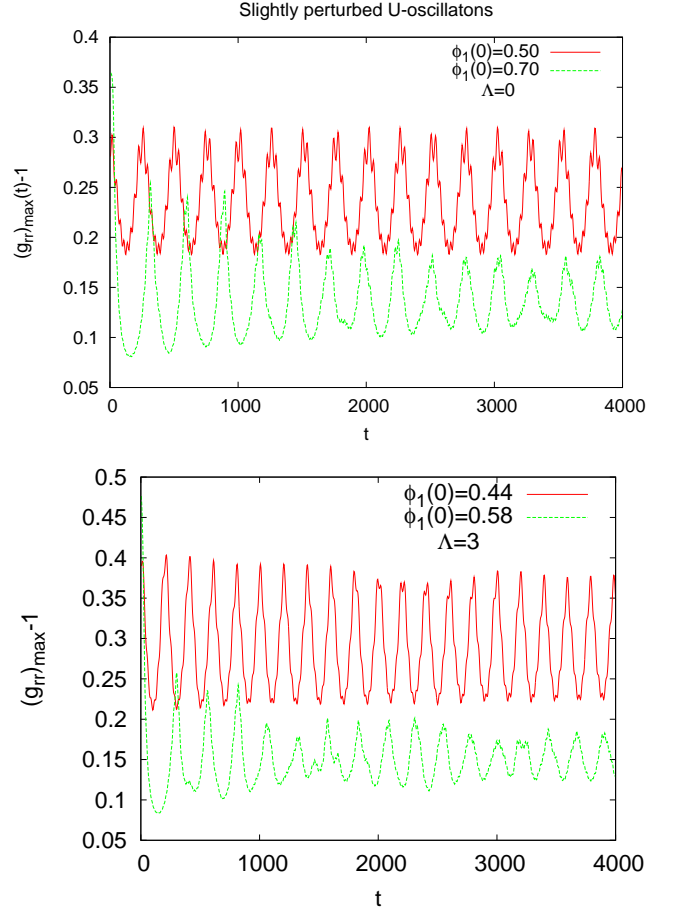


FIG. 15. Evolve profiles of the maximum value of the radial metric function g_{rr} for the slightly perturbed configurations: $\phi_1(0) = 0.5$ and $\phi_1(0) = 0.7$

Fig. 17 shows the behavior of the metric functions g_{rr} and g_{tt} for the case of strongly perturbed U-oscillaton. In the plot for $\Lambda = 0$, we can see that g_{tt} shows the well known "collapse of the lapse", and g_{rr} shows the "grid stretching"; both phenomena signal the possible formation of a black hole. These behaviors are absent in the evolution of the metric functions for other values of Λ .

Migration of the strongly-perturbed U-oscillaton corresponding to $\phi_1(0) = 0.6$, with a mass decrease of 2%, towards a S-oscillaton. See also Fig. 18, where we show the evolved profile of the radial metric function g_{rr} of the $\phi_1(0) = 0.6$ -oscillaton migrating to the following S-branch configurations: $\phi_1(0) = 0.3$ for $\Lambda = 0$, $\phi_1(0) = 0.28$ for $\Lambda = 1$, $\phi_1(0) = 0.18$ for $\Lambda = 2$, and $\phi_1(0) = 0.12$ for $\Lambda = 3$.

6. The S-U transition point

We look carefully at the equilibrium configurations located nearby the critical configuration, i.e., the most

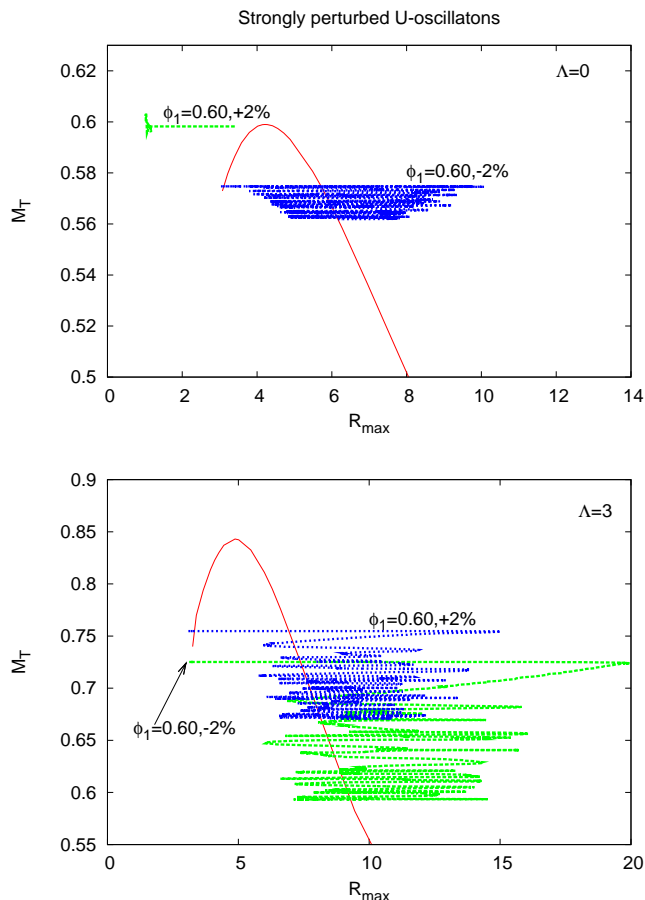


FIG. 16. Evolution of the perturbed configurations with $\phi_1(0) = 0.5$ and $\phi_1(0) = 0.6$ in a plot of M_T versus R_{max} . Only in the case of $\Lambda = 0$, both configurations collapse into a black hole if their mass is increased, even by a little. For other values of Λ , the larger values of the critical mass are able to prevent the collapse of the less perturbed of the configurations.

massive equilibrium configuration, see for instance Fig. 2, which is usually called the S-U transition point[3]. Fig. 19 shows the evolution of some slightly perturbed configuration near to the S-U transition point. With these examples we confirm previous results: S-oscillatons are intrinsically stable, whereas U-oscillatons are intrinsically unstable, no matter its proximity to the S-U transition point. Thus, this also confirms that the critical configuration is a true stability-instability transition point.

V. CONCLUSIONS

In this work, we solved numerically the Einstein-Klein-Gordon system for a massive and real scalar field endowed with a scalar potential containing a quartic self-interaction term. The diverse numerical experiments confirm the same general properties found in the case

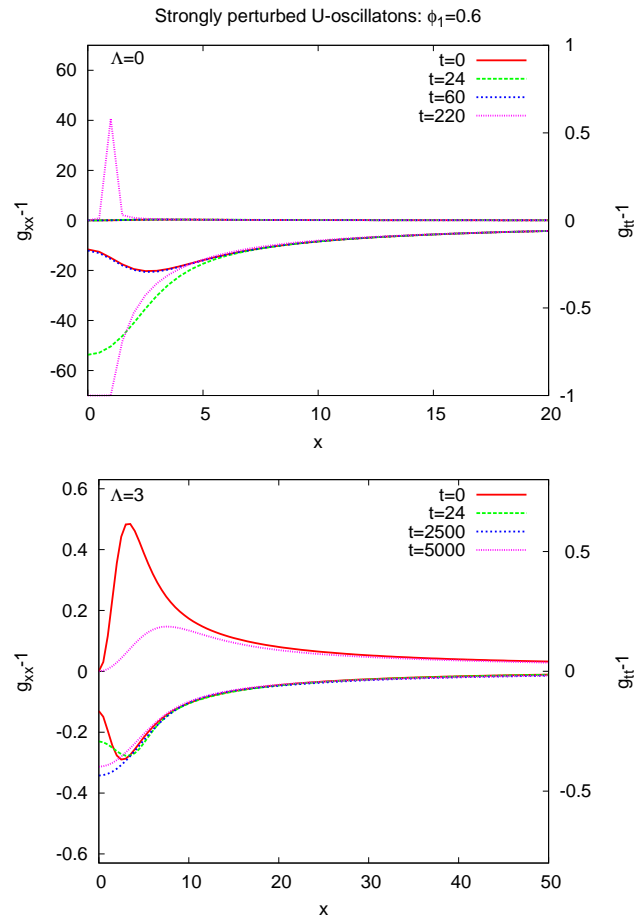


FIG. 17. Radial profiles of the metric functions g_{rr} and g_{tt} for a strongly-perturbed U-configuration corresponding to $\phi_1(0) = 0.6$ with an excess mass of 2%. The formation of a black hole seems to happen for $\Lambda = 0$, but its formation is prevented for other values.

of the free massive case, which are also present in the case of boson stars.

For all cases of the quartic self-interaction, it is found that there is a critical equilibrium configuration, which is the most massive one in each case; this critical configuration allows the separation of configurations into stable and unstable ones, the so-called S and U branches. As expected, the mass of the critical configuration increases for larger values of the quartic interaction.

Equilibrium configurations located on the S-branch are intrinsically stable, and vibrate with definite quasi-normal frequencies when slightly perturbed. If strongly perturbed, they can either migrate to another S-configuration, or collapse into a black hole, if its initial mass is smaller or larger, respectively, than the critical one. On the other hand, U-oscillatons are intrinsically unstable configurations. Under small perturbations, they are able to lose mass and migrate towards an equilibrium configuration on the S-branch, as long as its initial mass is not bigger than the critical one. However, un-

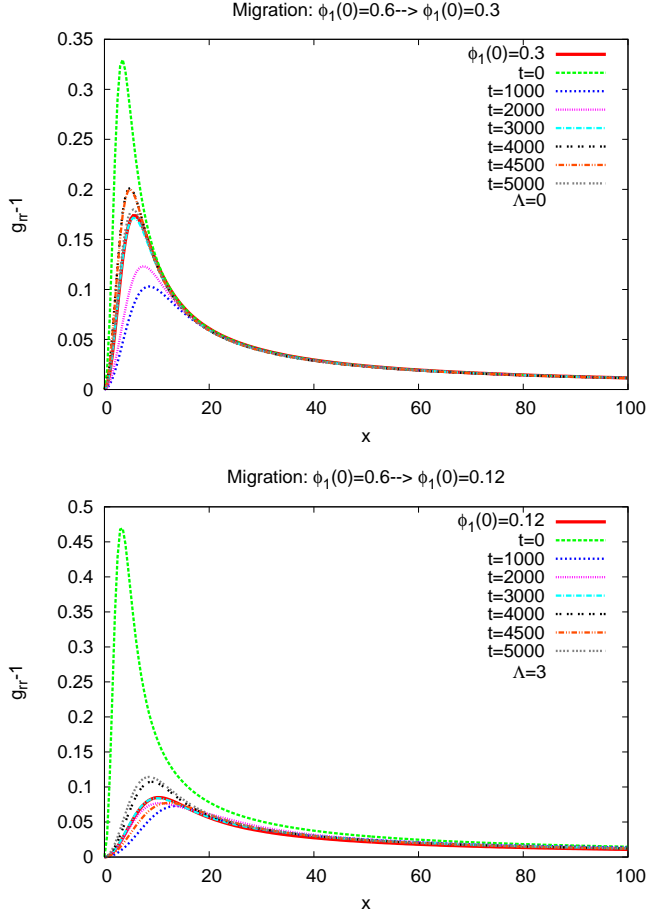


FIG. 18. The evolved profiles of the radial metric function g_{rr} of a perturbed U-oscillaton with $\phi_1(0) = 0.6$ and different values of Λ . In both cases, the evolution goes towards an equilibrium configuration in the S-branch.

der strong perturbations, U-oscillatons cannot prevent its collapse into black holes.

All in all, we have found that oscillatons with a quartic self-interaction share similar properties with their boson star counterparts. The larger the quartic interaction, the larger values the critical mass takes, but also the space for stable configurations is reduced because more diluted values of the scalar field are needed to sustain them. This can be seen in the shift of the critical scalar field value towards zero as the quartic interaction is increased.

It proved quite difficult to obtain equilibrium configurations for large values of the quartic interaction, because of the larger system of equations that must be solved in the case oscillatons (in terms of a Fourier expansion) as compared to the case of boson stars. Nonetheless, we have been able to explore the space parameter beyond the free case ($\Lambda = 0$), and provided evidence that points out to the close similarity of scalar configurations, whether

we speak of real or complex scalar fields.

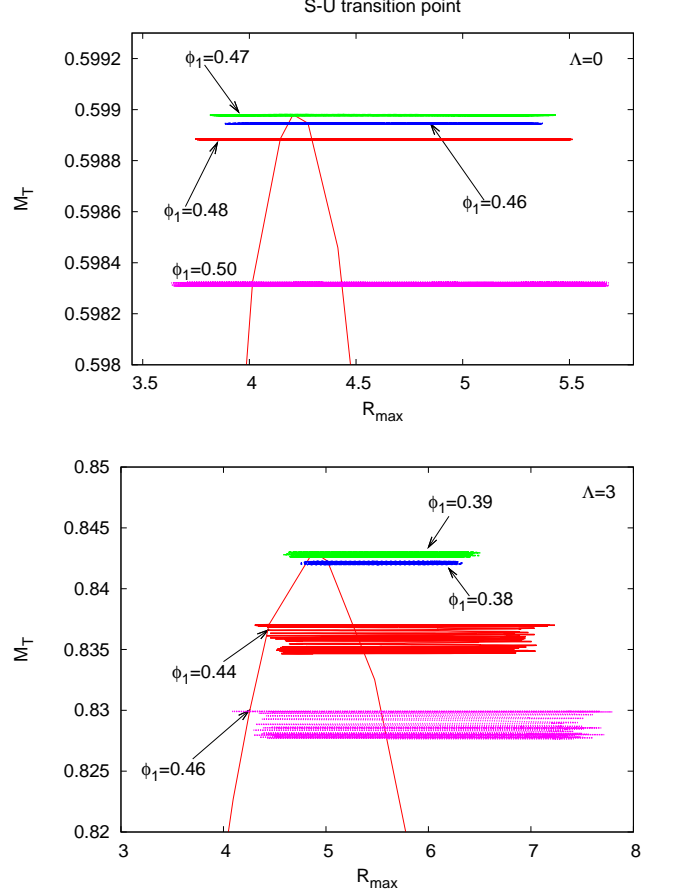


FIG. 19. Evolution of the slightly perturbed configuration near the S-U transition point. The nature of the transition point does not depend upon the value of Λ .

ACKNOWLEDGMENTS

SV-A thanks Carlos Palenzuela for useful comments, and acknowledges support from CONACyT, México, and the kind hospitality of the Canadian Institute for Theoretical Astrophysics (CITA), for a short research stay during which part of this work was done. RB acknowledges support from CONACyT, México under grants 83825. LAU-L thanks the Berkeley Center for Cosmological Physics (BCCP) for its kind hospitality, and the joint support of the Academia Mexicana de Ciencias and the United States-Mexico Foundation for Science for a summer research stay at BCCP. This work was partially supported by PROMEP, DAIP-UG, and by CONACyT México under grants 56946, and I0101/131/07 C-234/07 of the Instituto Avanzado de Cosmología (IAC) collaboration.

-
- [1] E. Seidel and W. M. Suen, Phys. Rev. Lett., **66**, 1659 (1991).
- [2] L. A. Urena-Lopez, T. Matos, and R. Becerril, Class. Quant. Grav., **19**, 6259 (2002).
- [3] M. Alcubierre *et al.*, Class. Quant. Grav., **20**, 2883 (2003), arXiv:gr-qc/0301105.
- [4] L. A. Urena-Lopez, Class. Quant. Grav., **19**, 2617 (2002), arXiv:gr-qc/0104093.
- [5] J. Balakrishna, R. Bondarescu, G. Daues, and M. Bondarescu, Phys. Rev., **D77**, 024028 (2008), arXiv:0710.4131 [gr-qc].
- [6] E. Seidel and W.-M. Suen, Phys. Rev. Lett., **72**, 2516 (1994), arXiv:gr-qc/9309015.
- [7] J. Balakrishna, R. Bondarescu, G. Daues, F. Siddhartha Guzman, and E. Seidel, Class. Quant. Grav., **23**, 2631 (2006), arXiv:gr-qc/0602078.
- [8] M. Colpi, S. L. Shapiro, and I. Wasserman, Phys. Rev. Lett., **57**, 2485 (1986).
- [9] F. S. Guzman, Phys. Rev., **D70**, 044033 (2004), arXiv:gr-qc/0407054.
- [10] P. Grandclement, G. Fodor, and P. Forgacs, (2011), arXiv:1107.2791 [gr-qc].
- [11] G. Fodor, P. Forgacs, and M. Mezei, Phys. Rev., **D82**, 044043 (2010), arXiv:1007.0388 [gr-qc].
- [12] G. Fodor, P. Forgacs, and M. Mezei, Phys. Rev., **D81**, 064029 (2010), arXiv:0912.5351 [gr-qc].
- [13] E. Masso, F. Rota, and G. Zsembinszki, Phys. Rev., **D72**, 084007 (2005), arXiv:astro-ph/0501381.
- [14] O. Obregon, L. A. Urena-Lopez, and F. E. Schunck, Phys. Rev., **D72**, 024004 (2005), arXiv:gr-qc/0404012.
- [15] T. Matos, J. A. Vazquez, and J. Magana, (2008), arXiv:0806.0683 [astro-ph].
- [16] D. N. Page, Phys. Rev., **D70**, 023002 (2004), arXiv:gr-qc/0310006.
- [17] F. S. Guzman and J. M. Rueda-Becerril, Phys. Rev., **D80**, 084023 (2009), arXiv:1009.1250 [astro-ph.HE].
- [18] A. Bernal and F. Siddhartha Guzman, Phys. Rev., **D74**, 103002 (2006), arXiv:astro-ph/0610682.
- [19] A. Bernal and F. S. Guzman, Phys. Rev., **D74**, 063504 (2006), arXiv:astro-ph/0608523.
- [20] J. Balakrishna, E. Seidel, and W.-M. Suen, Phys. Rev., **D58**, 104004 (1998), arXiv:gr-qc/9712064.
- [21] E. Seidel and W.-M. Suen, Phys. Rev., **D42**, 384 (1990).
- [22] S. A. T. Wiliam H. Press and others., *Numerical Recipes in C: The Art of Scientific Computing*, 2nd ed. (Press Syndicate of the University of Cambridge, 1992).

